J Nanopart Res (2020) 22: 143
https://doi.org/10.1007/s11051-020-04855-1

RESEARCH PAPER

Adsorption of carbon dioxide on $Cu_xMg_y(BTC)_2$ MOFs: influence of Cu/Mg ratio

Mohammad W. Kadi · H.M. Abd El Salam · T. Zaki · Reda M. Mohamed

Received: 1 March 2020 / Accepted: 21 April 2020 / Published online: 29 May 2020

Abstract A series of bimetallic metal-organic frameworks ($Cu_xMg_y(BTC)_2$ MOFs) was synthesized. The as-produced MOFs were described utilizing different characterizations techniques. The dynamic adsorption efficiencies of the prepared MOFs toward the carbon dioxide (CO_2) from the nitrogen stream at separate temperatures and various total levels of flow were achieved including the evaluation of the suitable kinetic model. The results showed that copper ions could be substituted successfully by magnesium ions up to molar ratio 1:1 ($Cu_{1.5}Mg_{1.5}(BTC)_2$ MOF), without obvious deformation in the crystalline structure of the parent $Cu_3(BTC)_2.3H_2O$ (HKUST-1). In all of the as-synthesized MOFs, the introduction of magnesium ions to the context of Cu-BTC had accompanied changes in the morphological structure, porosity, and thermal behavior. The $Cu_{1.5}Mg_{1.5}(BTC)_2$ MOF showed significant enhancing on its CO_2 adsorption capacity (23.85 mmol/g) compared with Cu-BTC MOF (5.95 mmol/g) and Mg-BTC MOF (4.57 mmol/g), which indicated the key-role of the central metals in the MOF in CO_2 adsorption. The second-order kinetic studies suited the experimental work with more precise than pseudo-first-order. Also, the reusability of the bimetallic adsorbent under the optimum temperature and flow rate was evaluated for 5 cycles.

Keywords Metal-organic frameworks, MOFs · $Cu_3(BTC)_2$ · $Cu_{1.5}Mg_{1.5}(BTC)_2$ · $Mg_3(BTC)_2$ · Carbon dioxide · Adsorption

This article is part of the topical collection: Nanotechnology in Arab Countries

Guest Editor: Sherif El-Eskandarany

Electronic supplementary material The online version of this article (https://doi.org/10.1007/s11051-020-04855-1) contains supplementary material, which is available to authorized users.

M. W. Kadi · R. M. Mohamed (✉)
Department of Chemistry, Faculty of Science, King Abdulaziz University, P.O. Box 80203, Jeddah 21589, Kingdom of Saudi Arabia
e-mail: redama123@yahoo.com

H. A. El Salam
Analysis and Evaluation Division, Egyptian Petroleum Research Institute, Nasr City, P.O. Box 11727, Cairo, Egypt

T. Zaki
Catalysis Department, Petroleum Refining Division, Egyptian Petroleum Research Institute, Nasr City, Nasr City, P.O. Box 11727, Cairo, Egypt

T. Zaki (✉)
EPRI Nanotechnology Center, Egyptian Petroleum Research Institute, Nasr City, Nasr City, P.O. Box 11727, Cairo, Egypt
e-mail: tamer_zaki_sharara@epri.sci.eg

e-mail: tamerzakisharara@yahoo.com

Introduction

Global warming has a calamitous impact that influences human potential. The emission of greenhouse gases (GHGs) like carbon dioxide (CO_2) is considered the main cause of climate change for many decades (Zaki 2020). Nowadays, the global sales for the adsorbents, in

the different industrial areas, exceed 10 billion USD. A huge dominate, motivate scientists worldwide to develop new materials having superior adsorption features (Hu et al. 2019). Metal-organic frameworks (MOFs), which are classified as coordinated networks or coordinated polymers (Satheesh et al. 2016), are distinguished by the soaring surface structure and tunability (Satheesh et al. 2016). The superior characteristics of MOFs directed the researches to evaluate its efficiencies in different applications such as the adsorption processes in the different fluids, the catalytic reactions either conventional or photo, energy storage, gas sensing, and drug delivery (Hossain et al. 2019). Recently, extensive studies were attained in carbon dioxide's capturing research via the adsorption on metal-organic frameworks (MOFs) (Liu et al. 2019), such as Cu-BTC (Liu et al. 2019; Li et al. 2014; Zhao et al. 2014 and Mua et al. 2018), MOFs-177 (Zn) (Millward and Yaghi 2005), MOF-74 (Mg, Co, Ni, Zn) (Bao et al. 2011 and Chaemchuen et al. 2013), MOF-210 (Furukawa et al. 2010), and Mg-DOBDC (Liu et al. 2016). Most of the released reports attributed the high efficiencies of MOF materials to the types of metals and linkers (Elsabawy and Fallatah 2019). However, at low-pressure circumstances like the atmospheric pressure, the weak interactive forces between the active sites and the carbon dioxide species decrease the capabilities of MOFs to capturing the CO_2 molecules in its required high performance (Ullah et al. 2020). Accordingly, numerous works were concerned with enhancing the adsorption capacity and discrimination of the parental MOFs concerning the CO_2 via different strategies such as modifying the crystal structure (Landaverde-Alvarado et al. 2017) or by changing the chemical features via carbonization (Kukulka et al. 2019), functionalization (Wang et al. 2014; Yan et al. 2014; Wang et al. 2015; Tari et al. 2016; Flaig et al. 2017; Fei et al. 2017; Su et al. 2017; Sun et al. 2018, and Li et al. 2020), cation doping (Koh et al. 2013; Zhou et al. 2016), or synthesizing MOF-composites (Bian et al. 2014; Xin et al. 2016; Moon et al. 2016; Chen et al. 2017a, b; Szczęśniak and Choma 2020, and Majumdar et al. 2020). A few types of research concerned with the performance of bimetallic MOFs to the adsorption of CO_2 (Gotthardt et al. 2015; He et al. 2020). He et al. 2020 found that the partial substitution of $Cu_3(BTC)_2.3H_2O$ MOF (known as HKUST-1) by Mg ions (Cu:Mg = 10:1) improved the surface properties of the Cu-BTC MOF that subsequently enhances its adsorption efficiency. To the best of our knowledge, the influence of increasing the ratio of doped magnesium in the framework of the HKUST-1 in its structure and adsorption efficiency is not explored yet. In this work, copper MOFs substituted with higher percentages of magnesium ions, i.e., higher than 10%, were prepared. This research aims to appraise the impact of such synthesis-route to the physical, chemical, and CO_2 adsorption capacities of the resulted products.

Experimental

Production and depiction of $Cu_xMg_y(BTC)_2$ samples

The synthesis procedures and categorization of the produced MOFs are presented in detail in the accompanying supplementary materials file.

Adsorption experiments of CO_2

The adsorption of CO_2 was investigated utilizing a homemade revolution curve machine. The apparatus contains a U-type glass column having a total stretch of 52 cm and a diameter of 1.2 cm. The column was dosen with 1 g of adsorbent. The active adsorption capability was measured by applying a gas mixture constituted of 15% CO_2 and 85% N_2. This mixture can be considered a standard model in industrial power plants. The adsorption measurements were achieved at 25, 50, and 75 °C and total flow rates of 40, 70, and 100 mL min^{-1}. Before each adsorption experiment, the MOF sample was in situ dried under a stream of nitrogen gas of 40 mL min^{-1} at 120 °C for 1 h. To investigate the reusability efficiency, the spent sample was heated at 120 °C for 3 h under a stream of nitrogen gas of 40 mL min^{-1} before each cycle. The gas evolved of the column's inlet and outlet was examined with a Hewlett Packard Gas Chromatograph (HP 6890) equipped with TCD/FID on time.

Results and discussion

Materials depiction

The elemental analysis of the Cu1.5Mg1.5 MOF sample via Atomic absorption (A.A.) spectrometry and the elemental analysis revealed that it was comprised of 3.10 mol% copper and 3.14 mol% magnesium, which

gives Cu/Mg molar ratio (0.99) very near to the targeted value, i.e., 1. The composition analysis of the other CuMg samples is listed in Table 1, which indicated the success of magnesium incorporation. Figure 1 explains the XRD patterns of the synthesized Cu3Mg0 and Cu0Mg3 samples. The patterns suggested the accomplishment of synthesis compared with the formerly reported studies related to $Cu_3(BTC)_2.3H_2O$, also called HKUST-1 (Yan et al. 2014; Campello et al. 2015), and $Mg_3(BTC)_2$ (Mazaj et al. 2013 and Lestari et al. 2019a, b) that prepared via applying the traditional heating methods, while the pattern of Cu1.5Mg1.5 indicated that the substituted of copper species by magnesium did not alter the crystalline feature of HKUST-1 MOF. In addition to that, XRD patterns of the other prepared bimetallic MOF samples having distinct Cu/Mg molar ratios (Fig. S1) showed only the reflections characterize of HKUST-1 MOF, starting from Cu2.5Mg0.5 sample (Fig. S1.a) until the Cu2Mg1 sample (Fig. S1.b). However, the Cu1Mg2 sample (Fig. S1.c) showed the reflections characterize $Cu_3(BTC)_2.3H_2O$ and $Mg_3(BTC)_2$ MOFs. Finally, the pattern of Cu0.5Mg2.5 sample (Fig. S1.d) indicated a failure in the substitution process, whereas the reflections of $Mg_3(BTC)_2$ (Mazaj et al. 2013 and Lestari et al. 2019a, b), became predominant.

The TGA behaviors of the produced samples (Figs. 2 and S2) shed light on the gradual changes in its thermal performances, coinciding with the increment of the doped percentages of magnesium from zero, i.e., HKUST-1 MOF (Cu3Mg0 sample, Fig. 2a), until the complete change of the profile to become more stable as in the magnesium MOF (Fig. 2c).

The TGA profile of the Cu3Mg0 sample (Fig. 2a) displayed two weight-loss actions. The first step launched at 35 °C and completed at 200 °C relates to the loss of physisorbed water and organic solvent molecules (Schlichte et al. 2004). The second feature that appeared in the 315–420 °C range can be ascribed to the breakdown of the metal-organic arrangement with a full conversion to CuO (Schlichte et al. 2004 and Najafi Nobar and Farooq 2012). By doping magnesium cations in the structure instead of copper with ratio 1:1 (Fig. 2b), two weight loss steps appeared in the ranges of 290–390 °C and 540–650 °C, in addition to dehydration weight loss step that occurred before 120 °C. These two steps may be resulted from the destruction of the framework into CuO and MgO, respectively (Schlichte et al. 2004 and Najafi Nobar and Farooq 2012), and might indicate the difference of the thermal resistance of the same organic linker when the central cation changed. On the other hand, Fig. 2c, clarified the high thermal stability of the Cu0Mg3 sample up to 640 °C (Lestari et al. 2019a, b).

Upon the complete transformation of Cu3Mg0 and Cu0Mg3 samples into the oxide forms, the specimen lost around 60.94 and 51.10 wt%, continuously, which is in accord with the formerly issued thermal depiction for similar structures (Sanz et al. 2013; Kaur et al. 2019, and Coates 2000).

The IR spectra of all prepared samples (Figs. 3 and S3) showed bands in the region of 1400–1650 cm^{-1} that

Table 1 Chemical composition of the prepared samples

Sample code	$Cu_{(measured)}$ (mol%)	$Mg_{(measured)}$ (mol%)	$C_{(measured)}$ (mol%)	$O_{(measured)}$ (mol%)	$H_{(measured)}$ (mol%)	$(Cu/Mg)_{Theor.}$ molar ratio	$(Cu/Mg)_{measured}$ molar ratio
Cu3Mg0	2.99	–	18.03	39.00	39.98	–	–
Cu2.5Mg0.5	4.16	0.85	29.96	31.69	33.34	5.00	4.87
Cu2Mg1	3.68	1.82	33.18	31.48	29.84	2.00	2.02
Cu1.5Mg1.5	3.10	3.14	37.44	31.13	25.18	1.00	0.99
Cu1Mg2	2.20	4.50	40.01	31.03	22.26	0.50	0.49
Cu0.5Mg2.5	1.05	5.66	39.65	30.88	22.76	0.20	0.18
Cu0Mg3	–	6.62	39.80	31.00	22.58	–	–

$Cu_{(measured)}$ and $Mg_{(measured)}$ referred to the measured contents of copper and magnesium by A.A., respectively

$C_{(measured)}$, $O_{(measured)}$, and $H_{(measured)}$ referred to the measured contents of carbon, oxygen and hydrogen in the prepared samples, respectively

$(Cu/Mg)_{Theor.}$ referred to the expected molar ratio of copper to magnesium in the prepared samples

$(Cu/Mg)_{measured}$ referred to the molar ratio of copper to magnesium in the prepared samples that calculated based on the measured contents of copper and magnesium by A.A.

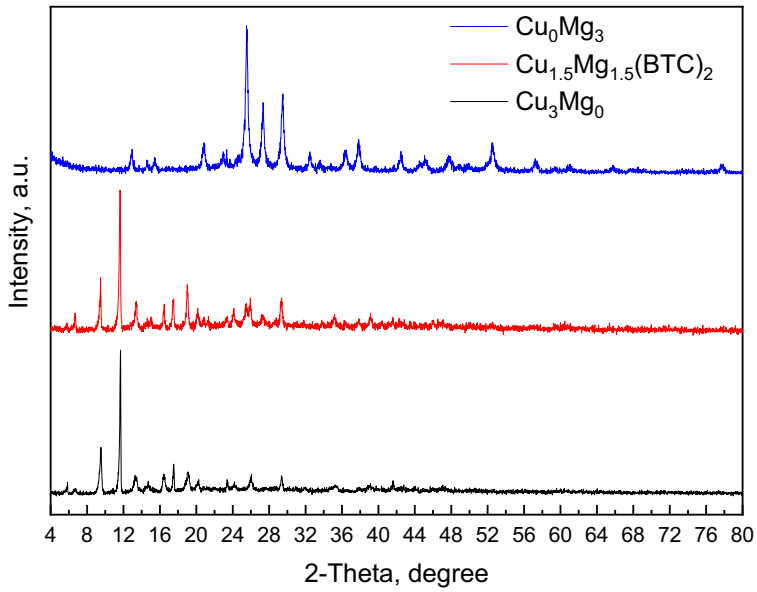

Fig. 1 X-ray diffraction patterns of Cu_3Mg_0, $Cu_{1.5}Mg_{1.5}(BTC)_2$, and Cu_0Mg_3 samples

ensued as of the symmetric and asymmetric vibrations of carboxylate functional groups (Chen et al. 2017a, b and Qian et al. 2012). The spectra indicated the removal of the residual non-reacted organic linker based on the absence of the bands characterize it in the range 1680–1750 cm^{-1} (Qian et al. 2012 and Lestari et al. 2019a, b). Also, the spectra clarified the bands around 600 cm^{-1} that may due to in- and out-of-plane deflection of $–CO_2$ groups (Pokhrel et al. 2018). In addition to that, the bands resulted from the stretching of C–O single bonds (Miller 2003) were found between 1250 and 1000 cm^{-1}. Finally, the stretching of C=C–C bonds in benzene tricarboxylate (Coates 2000) was represented by the bands at 750, 1000, and 1450–1510 cm^{-1}.

The Raman spectra of Cu3Mg0, Cu1.5Mg1.5, and Cu0Mg3 samples (Fig. S4) revealed the distinctive bands of metal species, (C–H) bending modes, (C=C) stretching modes, and symmetric and asymmetric extending of the carboxylates. The explanation of the Raman spectra is discussed in the supplementary materials.

All prepared MOF samples displayed type (IV) IUPAC for nitrogen adsorption-desorption isotherm, which characterizes the mesoporous materials that have to some extent micropores within its surfaces (Fig. 4 and Fig. S5). Table 2 demonstrates that Cu3Mg0 has the

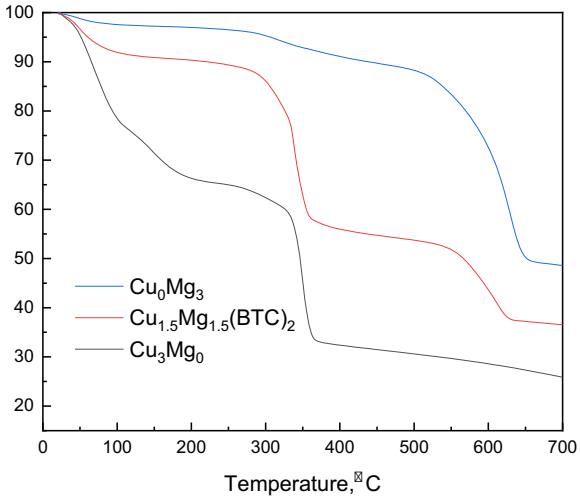

Fig. 2 TGA profiles of Cu_3Mg_0, $Cu_{1.5}Mg_{1.5}(BTC)_2$, and Cu_0Mg_3 samples

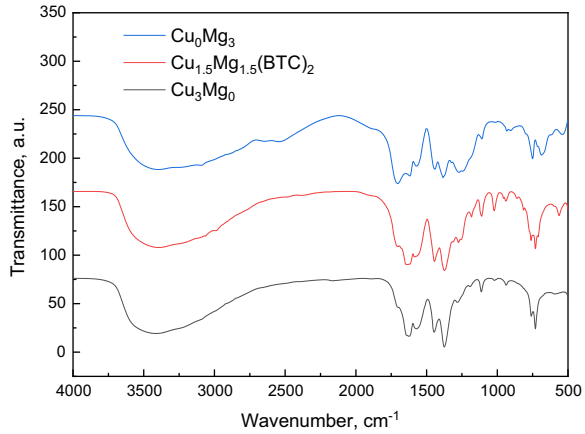

Fig. 3 FTIR spectra of Cu_3Mg_0, $Cu_{1.5}Mg_{1.5}(BTC)_2$, and Cu_0Mg_3 samples

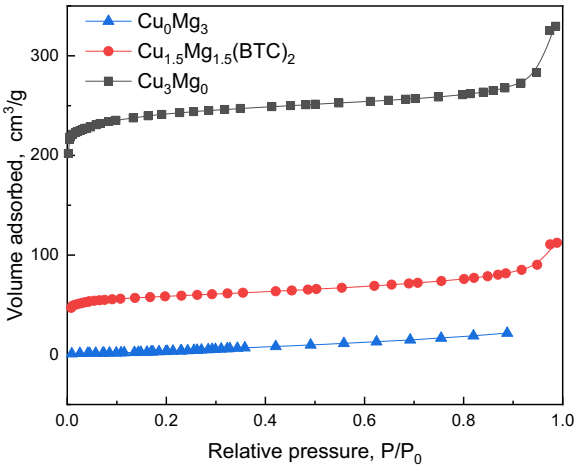

Fig. 4 Nitrogen adsorption-desorption isotherms of Cu_3Mg_0, $Cu_{1.5}Mg_{1.5}(BTC)_2$, and Cu_0Mg_3 samples

largest particular surface area (961.2 m^2 g^{-1}), which is comparable with the previous reports (Coates 2000). While Cu0Mg3 has the smallest specific surface area (44.78 m^2/g). It should be noticed that the prepared $Mg_3(BTC)_2$ MOF has relatively high surface features comparing with the previously reported Mg_BTC MOFs' (Lestari et al. 2019a, b). The increase of the percentage of the magnesium metal doping decreased gradually the surface area of the samples from 727.1 m^2 g^{-1} (Cu2.5Mg0.5 sample) to 45.56 m^2 g^{-1} (Cu0.5Mg2.5 sample) and subsequently the pore volume from 0.408 to 0.080 cm^3 g^{-1} for the same samples successively. This comportment agrees also with the prior studies for HKUST-1 MOF doped by other metals such as Ni/Cu BTC (Lin et al. 2014; Hu et al. 2014, and Abd El Salam et al. 2017) and Co/Cu BTC (Tian et al. 2019).

Table 2 Textural properties of the prepared samples

Sample code	S_{BET} (m^2/g)	S_{micro} (m^2/g)	V_p (cm^3/g)	D_H (nm)
Cu3Mg0	961.2	493.9	0.510	2.12
Cu2.5Mg0.5	727.1	561.5	0.408	2.22
Cu2Mg1	593.3	430.2	0.329	2.24
Cu1.5Mg1.5	227.2	97.96	0.174	3.06
Cu1Mg2	58.84	5.79	0.089	6.04
Cu0.5Mg2.5	45.56	2.55	0.080	7.07
Cu0Mg3	44.78	0.56	0.043	7.14

BET surface area (S_{BET}), micropores surface area (S_{micro}), total pore volume (V_p), and average pore diameter (D_H)

Figure 5 presents the SEM images attained for Cu3Mg0, Cu1.5Mg1.5, and Cu0Mg3. The distinguished octahedral shape of HKUST-1 MOF crystals is obvious in Fig. 5a (Huang et al. 2014). Upon substituting the copper species by magnesium ones, the crystals of the as-synthesized Cu1.5Mg1.5 MOF lost its regular shape and directed to be spherical (Fig. 5b). The absence of any octahedral crystals indicated the presence of one phase and the succeeding of the substitution step. On the other hand, the SEM image of Cu0Mg3 (Fig. 5c) illustrated the hollow spherical shape of $Mg_3(BTC)_2$ MOF (Lestari et al. 2019).

TEM images (Fig. 6) confirmed the related observations of SEM images (Fig. 5) for the samples Cu3Mg0, Cu1.5Mg1.5, and Cu0Mg3, where Fig. 6a showed the hexagonal shape, which can be defined as a perpendicular prediction of the double octahedral crystals of the copper MOF (Fig. 6a), while TEM images of doped copper MOF and magnesium MOF showed similar spherical aggregates (Fig. 6 b and c).

All of the previously mentioned characterizations, for the samples coded Cu2.5Mg0.5, Cu2Mg1, and Cu1.5Mg1.5 indicated, obviously, the success of the magnesium substitution process within the framework of the parent HKUST-1. Such success could be attributed to the vigorous preparation conditions concerning the previously reported conditions (Liu et al. 2018).

Evaluation and optimization of CO_2 adsorption

Figure 7 and Fig. S6 showed the results of carbon dioxide dynamic adsorption experiments for the differently prepared samples under the total flow rate of 40 mL/min and at temperature 25 °C. In general, the curves indicated the achieving of the mass transfer resistance phenomenon as the CO_2 being adsorbed. Whereas, the analysis of the outlet stream did not record carbon dioxide for a certain time according to the adsorption efficiency of the sample. After the saturation of the adsorbent bed, the concentration of carbon dioxide in the outlet stream started to increase gradually to form the breakthrough curve.

The adsorption capacities of the different MOFs were calculated based on the accumulated adsorbed amounts for 120 min.

Figure 7 clarified the obvious high efficiency of Cu1.5Mg1.5 (23.83 mmol CO_2/g) for its parent MOFs Cu3Mg0 (5.95 mmol CO_2/g) and Cu0Mg3 (4.66 mmol CO_2/g). On the other hand, Fig. S6 indicated the

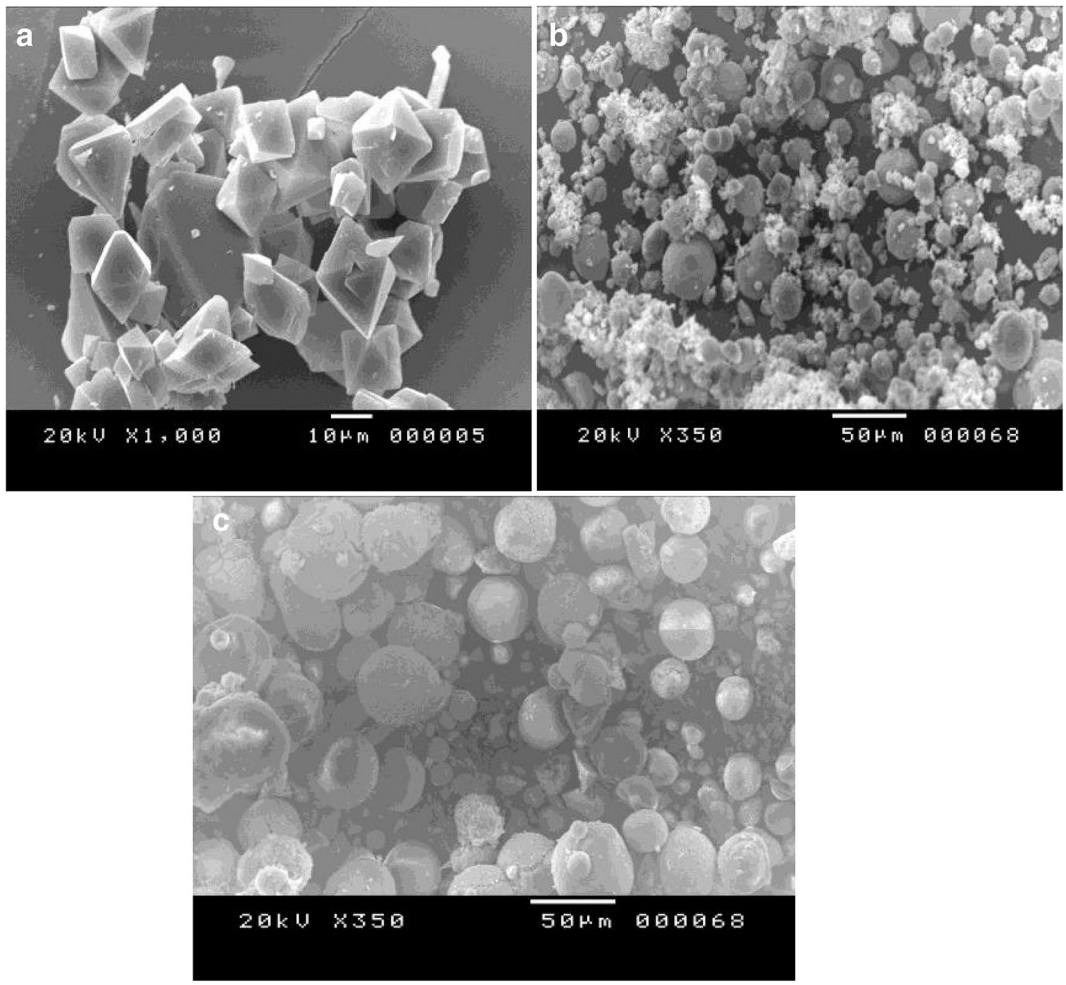

Fig. 5 SEM images of Cu_3Mg_0 (**a**), $Cu_{1.5}Mg_{1.5}(BTC)_2$ (**b**), and Cu_0Mg_3 (**c**) samples

adsorption capacity of the produced samples increased as the percentage of the doped magnesium increased, whereas the adsorption capacity of Cu3Mg0 increased to be 5.97 and 10.96 mmol CO_2/g for Cu2.5Mg0.5 and Cu2Mg1 samples, respectively. But, such activities started to decrease for sample Cu1Mg2 (19.86 mmol CO_2/g) and successively sample Cu0.5Mg2.5 (17.03 mmol CO_2/g) the highest active sample Cu1.5Mg1.5 (23.83 mmol CO_2/g).

The previously mentioned experimental data results may indicate that there is a particular doping percentage for the substitution of magnesium ions in the bimetallic Cu-Mg MOF for optimization of CO_2 adsorption efficiency via the influence on the location and arrangement of the up-taken CO_2 molecules.

Generally, the CO_2 adsorption progression mainly depends on two actions. The first is the strong Lewis acid and Lewis base reactions over both oxygens in CO_2 with the open metal ion sites (via the electrostatic interaction). The second is the carbon in CO_2 with organic ligands located at the cage window sites (via van der Waals forces) (Hou et al. 2013). It is well known that the interface between CO_2 quadrupole and metal vacancy position is stronger than the interaction with the cage window sites (Zhou et al. 2011). Accordingly, the efficiency of CO_2 adsorption could be adjusted via the electrostatic interaction strengths by changing metal atoms (Yu et al. 2013). The substitution of copper species of atomic radius 128 pm by larger ions of magnesium of atomic radius 173 pm may lead to electrostatic unbalance in the surface of the MOF, which motivate the adsorption efficiency due to the created synergetic phenomenon. Such influence started to decrease as the substitution of magnesium species

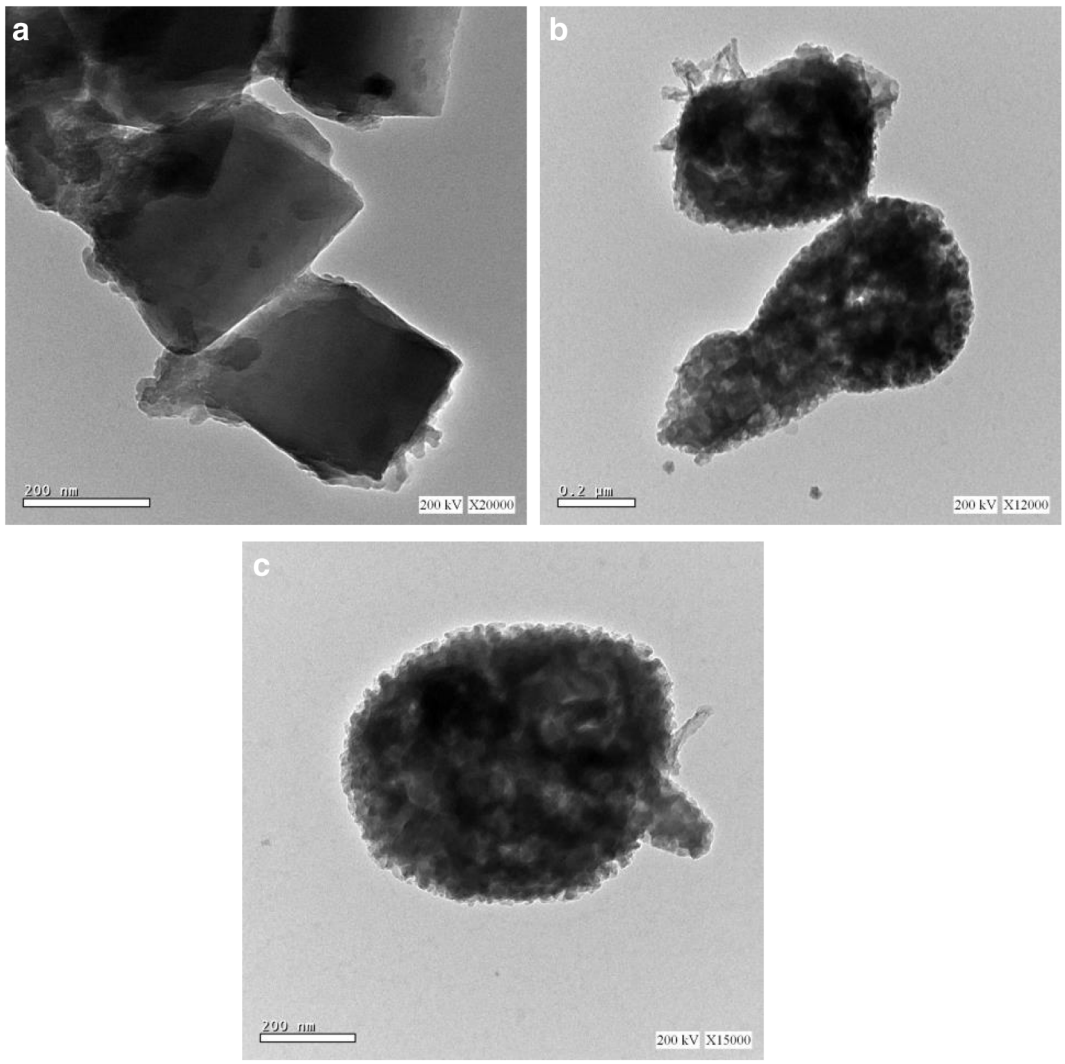

Fig. 6 TEM images of Cu_3Mg_0 (**a**), $Cu_{1.5}Mg_{1.5}(BTC)_2$ (**b**), and Cu_0Mg_3 (**c**) samples

exceeded 50% and became the predominant cation. Whereas, due to the big atomic radius of the magnesium, the electrostatic forces among the metal ions and CO_2 started to be weaker gradually as the magnesium wt% increase until it reached 100%.

Figure 8 clarified the influence of the stream flow rate on the adsorption efficiencies of the highest active sample, i.e., sample Cu1.5Mg1.5 (23.83 mmol CO_2/g). It is clear that as the inlet flow rate increase, the up-taking efficiency decrease, and the breakthrough time became shorter, which may be attributed to decreasing the contact time between the active sites and the adsorbate species.

The adsorption efficiency of the Cu1.5Mg1.5 sample decreased with increasing the temperature of the adsorption bed (Fig. 9). This may indicate the physical spirit of the adsorption progression on the MOF skim. In the physical adsorption, the electrostatic or the van der Waals interactions are playing the main roles (Zhao et al. 2013). Accordingly, the higher the temperatures, the CO_2 molecules gained enough energy to overcome the physical forces like the van der Waals and subsequently desorbed again to the gas stream (Simon et al. 2015; Borhan et al. 2019).

Several researches have studied CO_2 adsorption on $Cu_3(BTC)_2.3H_2O$ and its derivatives (Liu et al. 2013; Zhu et al. 2016). Regarding the updated literature survey, there no published work concerned with the carbon dioxide adsorption on $Mg_3(BTC)_2$. However, several works had focused on Mg-MOF-74 and its composites (Qasem and Ben-Mansour 2018). Only one research work had

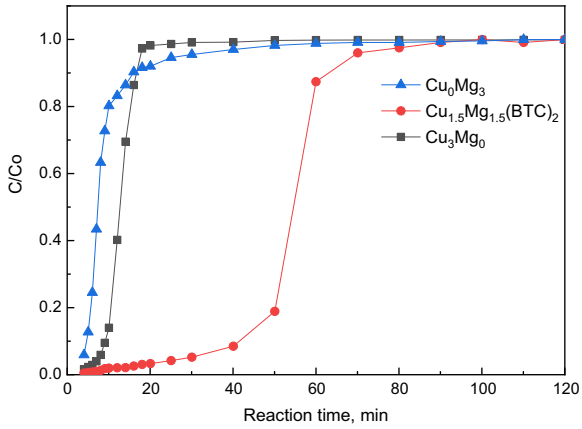

Fig. 7 CO_2 adsorption breakthrough curves on Cu_3Mg_0, $Cu_{1.5}Mg_{1.5}(BTC)_2$, and Cu_0Mg_3 samples, under the following adsorption conditions: bed temperature, 25 °C; total flow rate, 40 mL/min; CO_2, 15 Vol%

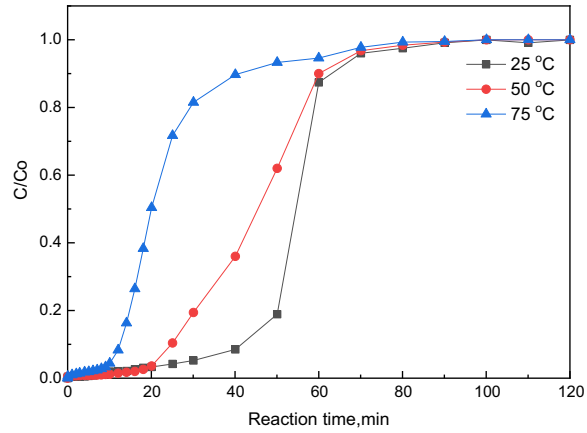

Fig. 9 CO_2 adsorption breakthrough curves on $Cu_{1.5}Mg_{1.5}(BTC)_2$ sample at different bed temperature, under the following adsorption conditions: total flow rate, 40 mL/min; CO_2, 15 Vol%

been achieved regarding the adsorption activity of Cu-Mg MOF but with a low doping percentage of magnesium.

The optimum CO_2 adsorption capacities that had been mentioned in all of the previously mentioned research works are listed for comparison versus the results obtained in this work (Table S1). As far as we know, this adsorption capacity of Cu1.5Mg1.5 sample at the optimum experimental conditions is the highest, regarding the measured activities for copper and magnesium MOFs and its derivatives.

Adsorption kinetics

The adsorption kinetic experiments offer vital evidence to expect the adsorption process. Consequently, the CO_2 capturing by Cu1.5Mg1.5 sample as a function of time, temperatures, and flow rates were examined by two nonlinear kinetic models, namely, pseudo-first-order (PFOM) and pseudo-second-order (PSOM) (Serna-Guerrero and Sayari 2010 and Rehman et al. 2019). The approximate kinetic constants are tabulated in Table 3.

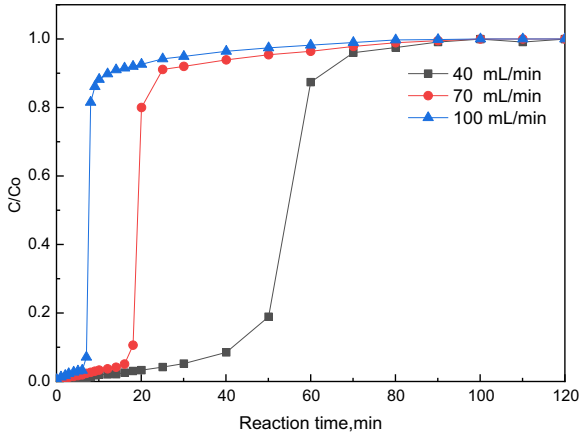

Fig. 8 CO_2 adsorption breakthrough curves on $Cu_{1.5}Mg_{1.5}(BTC)_2$ sample at different total inlet-stream flow rate, under the following adsorption conditions: bed temperature, 25 °C; CO_2, 15 Vol%

The nonlinear PFOM is expressed as

$$q_t = q_e(1-\exp(-K_1 t)) \quad (1)$$

The nonlinear POSM is given by

$$q_t = {}^{K_2 q_e^2 t}\!/_{1+K_2 q_e t} \quad (2)$$

where K_1 and K_2 are the pseudo-first- and second-order rate constants, q_e and q_t are the quantities of CO_2 adsorbed at equilibrium (mmol/g) and time t (min), individually.

Based on the coefficients (R^2) value, it is apparent that the PSOM is the finest, and the model could describe the adsorption of CO_2 by Cu1.5Mg1.5 sample better than PFOM with $R^2 > 0.99$ and $R^2 > \sim 0.98$ values through the different flow rates of the inlet stream (Fig. S7) and the different adsorption temperatures (Fig. S8), respectively.

Also, $q_{e,\ calc}$ the PSOM was closer to the investigational values of the equilibrium adsorption capacity, $q_{e,\ exp}$, than that of the PFOM. These outcomes confirmed that the PSOM was an extremely agreeable model to signify the CO_2 uptake by bimetallic MOF adsorbent, which may indicate the interaction of carbon dioxide

Table 3 Kinetic parameters for CO_2 adsorption on Cu1.5Mg1.5 sample

Inlet-stream total flow rate (mL/min)	$q_{e,exp}$ (mmol/g)	Pseudo-first-order model			Pseudo-second-order model		
		q_e (mmol/g)	k_1 (min^{-1})	R^2	q_e (mmol/g)	k_2 ($g.mmol^{-1}\ min^{-1}$)	R^2
40	23.83	22.96	0.0361	0.9651	24.07	0.0004	0.9995
70	17.57	19.04	0.0424	0.9462	16.98	0.0018	0.9950
100	11.71	9.54	0.0414	0.9410	10.98	0.0058	0.9765
Adsorption temperature (°C)	$q_{e,exp}$ (mmol/g)	Pseudo-first-order model			Pseudo-second-order model		
		q_e (mmol/g)	k_1 (min^{-1})	R^2	q_e (mmol /g)	k_2 ($g\ mmol^{-1}\ min^{-1}$)	R^2
25	23.83	22.96	0.0361	0.9651	24.07	0.0004	0.9995
50	19.64	24.41	0.0467	0.9361	19.87	0.0007	0.9994
75	10.79	9.54	0.0461	0.9829	10.44	0.0028	0.9963

molecules with different active sites in the MOF structure (Heydari-Gorji and Sayari 2011).

Reusability of the adsorbent

Figure S9 showed the results of carbon dioxide dynamic adsorption experiments. The high efficiency through the successive 5 cycles may be attributed to the substituted magnesium ions that have small electronegativity than the copper ions and subsequently, may adjust the carbon dioxide isosteric heat of adsorption, which mainly contributes in the regeneration development.

Conclusion

Magnesium-ion doping of HKUST-1 has been effectively accomplished up to molar ratio 1:1. The structures of the parent MOFs and the bimetallic MOFs were validated by numerous characterizations. $Cu_{1.5}Mg_{1.5}(BTC)_2$ achieved the highest adsorption capacity for the carbon dioxide molecules (23.85 mmol/g) from a binary gas stream (CO_2:N_2 = 15:85) of total flow rate 40 mL/min and at bed temperature 25 °C. The adsorption efficiency of $Cu_{1.5}Mg_{1.5}(BTC)_2$ MOF that based on the physical route could be credited to the synergistic impact of copper and magnesium ions on the carbon dioxide molecules.

Funding information This project was funded by the Deanship of Scientific Research (DSR) at the King Abdulaziz University, Jeddah, Saudi Arabia under grant no. D-530-130-1441. The authors, therefore, acknowledge with thanks DSR for the technical and financial support.

Compliance with ethical standards

Conflict of interest The authors declare that they have no conflict of interest.

References

Borhan A, Yusup S, Lim JW, Show PL (2019) Characterization and modelling studies of activated carbon produced from rubber-seed shell using KOH for CO_2 adsorption. Processes 7:855

Heydari-Gorji A, Sayari A (2011) CO_2 capture on polyethylenimine-impregnated hydrophobic mesoporous silica: experimental and kinetic modeling. Chem Eng J 173:72–79

Rehman A, Farrukh S, Hussain A, Fan X, Pervaiz E (2019) Adsorption of CO_2 on amine-functionalized green metal-organic framework: an interaction between amine and CO_2 molecules. Environ Sci Pollut Res 26:36214–36225

Millward AR, Yaghi OM (2005) Metal−organic frameworks with exceptionally high capacity for storage of carbon dioxide at room temperature. J Am Chem Soc 127(51):17998–17999

Szczęśniak B, Choma J (2020) Graphene-containing microporous composites for selective CO_2 adsorption. Microporous Mesoporous Mater 292:109761

Wang B, Huang H, Lv X-L, Xie Y, Li M, Li J-R (2014) Tuning CO_2 selective adsorption over N_2 and CH_4 in UiO-67 analogues through ligand functionalization. Inorg Chem 53: 9254–9259

Chen C, Li B, Zhou L, Xia Z, Feng N, Ding J, Wang L, Wan H, Guan G (2017a) Synthesis of hierarchically structured hybrid materials by controlled self-assembly of metal-organic framework with mesoporous silica for CO_2 adsorption. ACS Appl Mater Interfaces 9(27):23060–23071

Landaverde-Alvarado C, Morris AJ, Martin SM (2017) A new class of metal-cyclambased zirconium metal–organic frameworks for CO_2 adsorption and chemical fixation. J CO2 Util 19:40–48

Xin C, Jiao X, Yin Y, Zhan H, Li H, Li L, Wei W (2016) Enhanced CO_2 adsorption capacity and hydrothermal stability of HKUST-1 via introduction of siliceous mesocellular foams (MCFs). Ind Eng Chem Res 55:7950–7957

Zhou C, Cao L, Wei S, Zhang Q, Chen L (2011) A first principles study of gas adsorption on charged Cu–BTC. Comput Theor Chem 976:153–160

Zhu C, Zhang Z, Wang B, Chen Y, Wang H, Chen X, Zhang H, Sun N, Wei W, Sun Y (2016) Synthesis of HKUST-1#MCF compositing materials for CO_2 adsorption. Microporous Mesoporous Mater 226:476–481

Qian D, Lei C, Hao G-P, Li W-C, Lu A-H (2012) Synthesis of hierarchical porous carbon monoliths with incorporated metal-organic frameworks for enhancing volumetric based CO_2 capture capability. ACS Appl Mater Interfaces 4(11): 6125–6132

Yu D, Yazaydin AO, Lane JR, Dietzel PDC, Snurr RQ (2013) A combined experimental and quantum chemical study of CO_2 adsorption in the metal–organic framework CPO-27 with different metals. Chem Sci 4:3544–3556

Tian F, Qiao C, Zheng R, Ru Q, Sun X, Zhang Y, Meng C (2019) Synthesis of bimetallic–organic framework Cu/Co-BTC and the improved performance of thiophene adsorption. RSC Adv 9:15642–15647

Miller FA (2003) Chapter 8. In: Mayo DW, Miller FA, Hannah RW (eds) Course Notes on the Interpretation of Infrared and Raman Spectra. Wiley, New Jersey, p 205

Furukawa H, Ko N, Go YB, Aratani N, Choi SB, Choi E, Yazaydin AÖ, Snurr RQ, O'Keeffe M, Kim J, Yaghi OM (2010) Ultrahigh porosity in metal-organic frameworks. Science 329(5990):424–428

Li H, Bonduris H, Zhang X, Ye Y, Alsalme A, Lin R-B, Zhang Z, Xiang S, Chen B (2020) A microporous metal-organic framework with basic sites for efficient C_2H_2/ CO_2 separation. J Solid State Chem 284:121209

Abd El Salam HM, Younis SA, Ali HR, Zaki T (2017) Statistical modeling and optimization of phenol adsorption from water by modified $Cu_3(BTC)_2$: kinetic, isotherm, and thermodynamic. Microporous Mesoporous Mater 241:210–217

Koh HS, Rana MK, Hwang J, Siegel DJ (2013) Thermodynamic screening of metalsubstituted MOFs for carbon capture. PCCP 15:4573–4581

Moon H-S, Moon J-H, Chun DH, Park YC, Yun YN, Sohail M, Baek K, Kim H (2016) Synthesis of $[Mg_2(DOBDC)(DMF)_2]$@polystyrene composite and its carbon dioxide adsorption. Microporous Mesoporous Mater 232:161–166

Cho H-Y, Yang D-A, Kim J, Jeong S-Y, Ahn W-S (2012) CO_2 adsorption and catalytic application of Co-MOF-74 synthesized by microwave heating. Catal Today 185:35–40

Coates J (2000) Interpretation of infrared spectra, a practical approach. In: Meyers RA (ed) Encyclopedia of analytical chemistry. Wiley, Chichester, pp 10815–10837

Hu J, Yu H, Dai W, Yan X, Hua X, Huang H (2014) Enhanced adsorptive removal of hazardous anionic dye "Congo red" by a Ni/Cu mixed-component metal–organic porous material. RSC Adv 4:35124–35130

Li J, Yang J, Li L, Li J (2014) Separation of CO_2/CH_4 and CH_4/N_2 mixtures using MOF-5 and $Cu_3(BTC)_2$. J Energy Chem 23(4):453–460

Pokhrel J, Bhoria N, Wu C, Reddy KSK, Margetis H, Anastasiou S, George G, Mittal V, Romanos G, Karonis D, Karanikolos GN (2018) Cu- and Zr-based metal organic frameworks and their composites with graphene oxide for capture of acid gases at ambient temperature. J Solid State Chem 266:233–243

Simon JC, Bushra AD, Nannan S, Cheng-gong S, Colin ES, Kaixi LS, Joseph W (2015) Carbon dioxide separation from nitrogen/hydrogen mixtures over activated carbon beads: adsorption isotherms and breakthrough studies. Energy Fuel 29:3796–3807

Schlichte K, Kratzke T, Kaskel S (2004) Improved synthesis, thermal stability and catalytic properties of the metal-organic framework compound $Cu_3(BTC)_2$. Microporous Mesoporous Mater 73:81–88

Elsabawy KM, Fallatah AM (2019) Synthesis of newly wings like structure non-crystalline Niþþ-1,3,5- tribenzyl-1,3,5-triazine-2,4,6-(1H,3H,5H)-trione coordinated MOFs for CO2-capture. J Mol Struct 1177:255–259

Mazaj M, ČeliČ TB, Mali G, Rangus M, KauČiČ V, Logar NZ (2013) Control of the crystallization process and structure dimensionality of Mg−benzene−1,3,5-tricarboxylates by tuning solvent composition. Cryst Growth Des 13:3825–3834

Sun M, Yan S, Sun Y, Yang X, Guo Z, Du J, Xing H (2018) Enhancement of visible light-driven CO_2 reduction performance using an amine-functionalized zirconium metal–organic framework. Dalton Trans 47:909–915

Gotthardt MA, Schoch R, Wolf S, Bauer M, Kleist W (2015) Synthesis and characterization of bimetallic metal–organic framework Cu–Ru-BTC with HKUST-1 structure. Dalton Trans 44:2052–2056

Hossain MI, Cunningham JD, Becker TM, Grabicka BE, Walton KS, Rabideau BD, Glover TG (2019) Impact of MOF defects on the binary adsorption of CO2 and water in UiO-66. Chem Eng Sci 203:346–357

Wang N, Mundstock A, Liu Y, Huang A, Caro J (2015) Amine-modified mg-MOF-74/CPO-27-mg membrane with enhanced H2/ CO_2 separation. Chem Eng Sci 124:27–36

Qasem NAA, Ben-Mansour R (2018) Adsorption breakthrough and cycling stability of carbon dioxide separation from CO_2/ N_2/ H_2O mixture under ambient conditions using 13X and Mg-MOF-74. Appl Energy 230:1093–1107

Tari NE, Tadjarodi A, Tamnanloo J, Fatemi S (2016) Synthesis and property modification of MCM-41 composited with Cu (BDC) MOF for improvement of CO_2 adsorption selectivity. J CO2 Util 14:126–134

Satheesh R, Vignesh K, Rajarajan M, Suganthi A, Sreekantan S, Kang M (2016) Removal of Congo red from water using quercetin modified α-Fe2O3 nanoparticles as effective nanoadsorbent. Mater Chem Phys 180:53–65

Kaur R, Kaur A, Umar A, Anderson WA, Kansal SK (2019) Metal organic framework (MOF) porous octahedral nanocrystals of Cu-BTC: synthesis, properties and enhanced adsorption properties. Mater Res Bull 109:124–133

Sanz R, Martinez F, Orcajo G, Wojtas L, Briones D (2013) Synthesis of a honeycomb-like Cu-based metal–organic framework and its carbon dioxide adsorption behaviour. Dalton Trans 42:2392–2398

Serna-Guerrero R, Sayari A (2010) Modeling adsorption of CO_2 on amine-functionalized mesoporous silica. 2: kinetics and breakthrough curves. Chem Eng J 161:182–190

Flaig RW, Osborn Popp TM, Fracaroli AM, Kapustin EA, Kalmutzki MJ, Altamimi RM, Yaghi OM (2017) The chemistry of CO_2 capture in an amine-functionalized metal–organic framework under dry and humid conditions. J Am Chem Soc 139:12125–12128

Chaemchuen S, Kabir NA, Zhou K, Verpoort F (2013) Metal-organic frameworks for upgrading biogas via CO_2 adsorption to biogas green energy. Chem Soc Rev 42(24):9304–9332

Lin S, Song Z, Che G, Ren A, Li P, Liu C, Zhang J (2014) Adsorption behavior of metal–organic frameworks for methylene blue from aqueous solution. Microporous Mesoporous Mater 193:27–34

Liu S, Sun L, Xu F, Zhang J, Jiao C, Li F, Li Z, Wang S, Wang Z, Jiang X, Zhou H, Yang L, Schick C (2013) Nanosized Cu-MOFs induced by graphene oxide and enhanced gas storage capacity. Energy Environ Sci 6:818–823

Majumdar S, Tokay B, Martin-Gil V, Campbell J, Castro-Muñoz R, Ahmad MZ, Fila V (2020) Mg–MOF–74/Polyvinyl acetate (PVAc) mixed matrix membranes for CO_2 separation. Sep Purif Technol 238:116411

Najafi Nobar S, Farooq S (2012) Experimental and modeling study of adsorption and diffusion of gases in Cu-BTC. Chem Eng Sci 84:801–813

Ullah S, Bustam MA, Al-Sehemi AG, Assiri MA, Abdul Kareem FA, Mukhtar A, Ayoub M, Gonfa G (2020) Influence of post-synthetic graphene oxide (GO) functionalization on the selective CO2/CH4 adsorption behavior of MOF-200 at different temperatures; an experimental and adsorption isotherms study. Microporous Mesoporous Mater 296:110002

Campello SL, Gentil G, Júnior SA, de Azevedo WM (2015) Laser ablation: a new technique for the preparation of metal-organic frameworks $Cu_3(BTC)_2(H_2O)_3$. Mater Lett 148: 200–203

Zaki T (2020) Application of metal-organic frameworks in carbon dioxide conversion to methanol, Chapter 3, pages 75–90, in Conversion of Carbon Dioxide into Hydrocarbons Vol. 2 Technology, ed. by Inamuddin, A.M. Asiri, Eric Lichtfouse, series: Environmental Chemistry for a Sustainable World, ed. by Eric Lichtfouse, Jan Schwarzbauer, Didier Robert, vol. 41, Springer Nature Switzerland AG, Switzerland, https://doi.org/10.1007/978-3-030-28638-5

Huang W, Zhou X, Xia Q, Peng J, Wang H, Li Z (2014) Preparation and adsorption performance of GrO@Cu-BTC for separation of CO_2/CH_4. Ind Eng Chem Res 53:11176–11184

Kukulka W, Cendrowski K, Michalkiewicz B, Mijowska E (2019) MOF-5 derived carbon as material for CO2 absorption. RSC Adv 9:18527–18537

Lestari WW, Tedra RA, Novita TH, Shahab S (2019a) The role of magnesium(II) salt precursor in controlling the structure of coordination polymers based on magnesium(II) and benzene 1,3,5-tricarboxylic acid, international conference on advanced materials for better future 2018. IOP Conf Series Mater Sci Eng 578:012075

Lestari WW, Shahab S, Novita TH, Tedra RA, Purnawan C, Arrozi USF, Ni'maturrohmah D (2019b) Electrosynthesis of coordination polymers containing magnesium(II) and benzene 1,3,5-tricarboxylate: the influence of solvents and electrolytes toward the dimensionality, 13th joint conference on chemistry. IOP Conf Ser Mater Sci Eng 509:012149

He X, Chen D-R, Wang W-N (2020) Bimetallic metal-organic frameworks (MOFs) synthesized using the spray method for tunable CO_2 adsorption. Chem Eng J 382:122825

Mua X, Chena Y, Lester E, Wua T (2018) Optimized synthesis of nano-scale high-quality HKUST-1 under mild conditions and its application in CO_2 capture. Microporous Mesoporous Mater 270:249–257

Su X, Bromberg L, Martis V, Simeon F, Huq A, Hatton TA (2017) Postsynthetic functionalization of Mg-MOF-74 with tetraethylenepentamine: structural characterization and enhanced CO_2 adsorption. ACS Appl Mater Interfaces 9: 11299–11306

Yan X, Komarneni S, Zhang Z, Yan Z (2014) Extremely enhanced CO_2 uptake by HKUST-1 metal–organic framework via a simple chemical treatment. Microporous Mesoporous Mater 183:69–73

Hou X-J, He P, Li H, Wang X (2013) Understanding the adsorption mechanism of C2H2, CO_2, and CH_4 in isostructural metal–organic frameworks with coordinatively unsaturated metal sites. J Phys Chem C 117:2824–2834

Chen Y, Lv D, Wu J, Xiao J, Xi H, Xia Q, Li Z (2017b) A new MOF-505@ GO composite with high selectivity for CO_2/CH_4 and CO_2/N_2 separation. Chem Eng J 308:1065–1072

Liu Y, Hu J, Ma X, Liu J, Lin YS (2016) Mechanism of CO_2 adsorption on Mg/DOBDC with elevated CO_2 loading. Fuel 181:340–346

Liu Y, Ghimire P, Jaroniec M (2019) Copper Benzene-1,3,5-Tricarboxylate (Cu-BTC) metal-organic framework (MOF) and porous carbon composites as efficient carbon dioxide adsorbents. J Colloid Interface Sci 535:122–132

Liu Y, Liu S, Gonçalves AAS, Jaroniec M (2018) Effect of metal–ligand ratio on the CO_2 adsorption properties of Cu–BTC metal–organic frameworks. RSC Adv 8:35551–35556

Zhao Y, Seredych M, Jagiello J, Zhong Q, Bandosz TJ (2014) Insight into the mechanism of CO_2 adsorption on Cu-BTC and its composites with graphite oxide or aminated graphite oxide. Chem Eng J 239:399–407

Zhao Y, Seredych M, Zhong Q, Bandosz TJ (2013) Superior performance of copper based MOF and aminated graphite oxide composites as CO_2 adsorbents at room temperature. ACS Appl Mater Interfaces 5:4951–4959

Bao Z, Yu L, Ren Q, Lu X, Deng S (2011) Adsorption of CO_2 and CH_4 on a magnesium-based metal-organic framework. J Colloid Interface Sci 353(2):549–556

Bian Z, Zhu X, Jin T, Gao J, Hu J, Liu H (2014) Ionic liquid-assisted growth of $Cu_3(BTC)_2$ nanocrystals on graphene oxide sheets: towards both high capacity and high rate for CO_2 adsorption. Microporous Mesoporous Mater 200:159–164

Hu Z, Wang Y, Shah BB, Zhao D (2019) CO2 capture in metal–organic framework adsorbents: an engineering perspective. Adv Sustainable Syst 3:1800080

Zhou Z, Mei L, Ma C, Xu F, Xiao J, Xia Q, Li Z (2016) A novel bimetallic MIL-101 (Cr, Mg) with high CO_2 adsorption capacity and CO_2/N_2 selectivity. Chem Eng Sci 147:109–117